# Perivascular macrophages mediate neutrophil recruitment during bacterial skin infection

**Arby Abtin**[1,*], **Rohit Jain**[1,*], **Andrew J. Mitchell**[1,*], **Ben Roediger**[1], **Anthony J. Brzoska**[2], **Shweta Tikoo**[1], **Qiang Cheng**[3], **Lai Guan Ng**[4], **Lois L. Cavanagh**[1,5], **Ulrich H. von Andrian**[6], **Michael J. Hickey**[3], **Neville Firth**[2], and **Wolfgang Weninger**[1,7,8]

[1]The Centenary Institute, Newtown, NSW 2042, Australia

[2]School of Biological Sciences, University of Sydney, NSW 2006, Australia

[3]Centre for Inflammatory Diseases, Monash University Department of Medicine, Monash Medical Centre, Clayton, VIC, Australia

[4]Singapore Immunology Network (SIgN), Agency for Science, Technology and Research (A*STAR), Biopolis, Singapore

[5]Sydney Medical School, 2006, NSW, Australia

[6]Immune Disease Institute and Division of Immunology, Department of Microbiology and Immunobiology, Harvard Medical School, Boston, MA 02115, USA

[7]Discipline of Dermatology, Sydney Medical School, 2006, NSW, Australia

[8]Department of Dermatology, Royal Prince Alfred Hospital, Camperdown 2050, NSW, Australia

## Abstract

Transendothelial migration of neutrophils in post-capillary venules is a key event in the inflammatory response against pathogens and tissue damage. The precise regulation of this process is incompletely understood. We report that perivascular macrophages are critical for neutrophil migration into skin infected with the pathogen *Staphylococcus aureus*. Using multiphoton intravital microscopy we show that neutrophils extravasate from inflamed dermal venules in close proximity to perivascular macrophages, which are a major source of neutrophil chemoattractants. The virulence factor alpha-hemolysin lyses perivascular macrophages leading to decreased neutrophil transmigration. Our data illustrate a previously unrecognized role for perivascular macrophages in neutrophil recruitment to inflamed skin, and indicate that

Corresponding author: Wolfgang Weninger, M.D., The Centenary Institute, Locked Bag No. 6, Newtown, NSW 2042, Australia, Phone: +61 2 9515 6861; Fax: +61 2 9656 1048; w.weninger@centenary.org.au.
*These authors contributed equally to this work

*Staphylococcus aureus* uses hemolysin-dependent killing of these cells as an immune evasion strategy.

## Introduction

Neutrophils, through their ability to be rapidly recruited to tissues and deploy a diverse array of antimicrobial effector mechanisms, are essential for the clearance of many bacterial pathogens[1]. Given the potentially logarithmic growth of microorganisms during early stages of infection, effective destruction of pathogens depends upon the timely coordination of a complex series of cellular and molecular processes within the host. This commences with immune 'sensing' of pathogens by tissue-resident cells followed by activation of the vascular endothelium and neutrophil extravasation from the bloodstream, and finally initiation of neutrophil antimicrobial functions[1, 2].

The current paradigm of neutrophil recruitment is described by a well-defined series of steps that occur within post-capillary venules[1, 3]. The first of these is tethering and rolling on the vascular endothelium, which is mediated by P-selectin glycoprotein ligand-1 (PSGL-1) or VLA-4 (very late antigen-4/CD49d/CD29) on the neutrophil and E- and P-selectin or VCAM-1 (vascular cell adhesion molecule) on the endothelium[4]. Under the influence of Gα-coupled chemokine receptor-mediated signaling, conformational changes in the β2 integrins LFA-1 and Mac-1 occur on rolling cells, resulting in increased integrin affinity for their endothelial ligands[5]. Subsequent to adhesion, neutrophils crawl along the intraluminal surface of the vessel in a Mac-1 dependent manner to reach a preferred site of transendothelial migration (TEM), which in some cases may be through the endothelial cell itself (transcellular pathway) but typically occurs between endothelial cell junctions (paracellular pathway)[6, 7].

Although the sequential model of leukocyte recruitment is well supported by many studies, recent findings have suggested that additional mechanisms coordinate this process, particularly in the perivascular space. Immediately following migration through the endothelial layer, neutrophils enter a space between endothelial cells and surrounding pericytes. Once there, they migrate along pericyte processes in a Mac-1/LFA-1/ICAM-1 dependent manner to reach optimal sites of exit from the pericyte layer[8]. In addition to pericytes, immune cell subpopulations, particularly macrophages[9–11], are associated with post-capillary venules. Based on their expression of a range of pattern recognition receptors and ability to produce pro-inflammatory cytokines and chemokines, tissue-resident macrophages have been argued to participate in the induction of inflammation[12]. Nevertheless, the precise role of macrophages, in particular the perivascular subset, on neutrophil recruitment during tissue inflammation, if any, is unclear.

Of the human pathogens that require neutrophils for control and clearance, infections with *Staphylococcus aureus* (*S. aureus)* are particularly prevalent, resulting in an estimated 1.3 million infections and 390,000 hospital admissions per year in the US alone[13, 14]. In addition, the widespread emergence of nosocomial and community-acquired methicillin-resistant (CA-MRSA) strains represents a major health problem, and it is estimated that the mortality due to MRSA infections is comparable to the combined total of AIDS,

tuberculosis and viral hepatitis[15]. The fact that most systemic sequelae caused by *S. aureus* originate from skin infections necessitates an in-depth understanding of the cutaneous anti-bacterial immune response.

A key virulence strategy used by many pathogens is to subvert effective immune responses. The pathogenicity of *S. aureus* is due, in large part, to a diverse array of virulence factors that strains may produce. Foremost amongst these is a range of cytotoxins that includes α-hemolysin (Hla), Panton Valentine Leukocidin and Phenol Soluble Modulins[16]. The secreted pore-forming cytolysin Hla, which is produced by virtually all clinical isolates, has been implicated in the pathogenesis of necrotising pneumonia and skin infections[17–20]. Hla binds to the membrane-associated protease A Disintegrin and Metallopeptidase 10 (ADAM10), which has been shown to facilitate Hla-mediated disruption of epithelial integrity[19–21]. However, whether and how Hla interferes with the ensuing innate immune response is incompletely understood.

Given that the precise cellular and molecular events that take place during early infection with *S. aureus* are ill-defined, we utilized our well-characterized intravital skin imaging model[22] in combination with fluorescently-tagged bacterial strains to dissect the orchestration of the cutaneous anti-bacterial immune response. We further made use of an isogenic deletional bacterial mutant that lacks functional Hla (ΔHla) to determine the actions of this essential virulence factor within the context of an intact microenvironment *in vivo*. When compared with wild-type (WT) *S. aureus*, infection with ΔHla *S. aureus* led to increased neutrophil recruitment, decreased bacterial load and protection from tissue necrosis. Strikingly, in ΔHla *S. aureus*-infected animals, neutrophils were found to preferentially extravasate from "hotspots" that were in close physical proximity to perivascular macrophages (PVM), which were the dominant source of neutrophil-attracting chemokines. In contrast, during infection with WT *S. aureus*, neutrophils failed to arrest on the inflamed endothelium and subsequently transmigrate, and this was associated with rapid, specific Hla-dependent lysis of PVM. Our studies reveal the thus far unknown guidance of blood-borne leukocytes during extravasation by perivascular hematopoietic cells and provide novel insight into the mechanisms of bacterial immunoevasion.

## Results

### Hla interferes with neutrophil accumulation during cutaneous *S. aureus* infection

While neutrophils are required for the control and clearance of bacterial infections, the mechanisms that regulate their homing from the bloodstream and subsequent interstitial migration at sites of bacterial barrier breach are incompletely understood. We have previously established the ear skin in mice as an ideal site for dissecting anti-pathogen responses, as resident immune cells are well defined and the ear is readily accessible for intravital imaging[22].

We initially compared the capacity of various bacteria to cause neutrophil influx into ear skin in order to assess potential strain-specific differences in this essential step of the immune response. We found that neutrophil numbers in skin infected with the commensal *S. epidermidis* and *E. coli* were significantly higher than that of WT *S. aureus* (Fig. 1a). Since

the virulence factor Hla has been implicated in the pathogenesis of cutaneous *S. aureus* infections, we determined neutrophil numbers following injection with *S. aureus* DU1090, which is an isogenic Hla-deficient strain (ΔHla). Remarkably, this resulted in neutrophil numbers similar to *S. epidermidis* and *E. coli* (Fig. 1a), indicating that Hla impacts on the accumulation of neutrophils in infected skin. Macroscopically, ears infected with ΔHla *S. aureus* showed more pronounced signs of inflammation as indicated by increased redness and ear thickness as compared to WT bacteria (Fig. 1b; Suppl. Fig. 1a). Furthermore, an increased number of red blood cells (RBC) was observed in the absence of Hla, consistent with the hemolytic activity of this virulence factor (Suppl. Fig. 1b). Co-injection of ΔHla *S. aureus* with purified Hla phenocopied infection with WT *S. aureus* (Suppl. Fig. 1c&d). Strikingly, over the course of several days, infection with WT *S. aureus* culminated in necrosis, while infection with ΔHla *S. aureus* ultimately resulted in complete reconstitution of tissue integrity (Fig. 1b).

To better understand these divergent outcomes, we conducted a detailed analysis of neutrophil influx into the skin during *S. aureus* infection. While no difference was observed at 4h post-infection (p.i.), significantly higher numbers of neutrophils accumulated in ΔHla *S. aureus* infected skin at 8h, 12h, 24h and 48h p.i. (Fig. 1c). These changes in absolute neutrophil number were corroborated by myeloperoxidase assays (Fig. 1d) and histopathology, which revealed increased ear thickness and large numbers of neutrophils in the dermis of mice infected with ΔHla *S. aureus* (Fig. 1e). Neutrophil recruitment was impeded when ΔHla *S. aureus* injection was combined with purified Hla (Fig. 1f). Treatment of WT *S. aureus* infected mice with Hla antiserum resulted in increased neutrophil numbers in the skin (Fig. 1g), while the antiserum had no effect in ΔHla *S. aureus*-infected mice (data not shown). These additional controls demonstrate that the phenotypic difference observed with ΔHla *S. aureus* was indeed due to the absence of Hla in the bacterium rather than some unrecognized changes mediated by genetic manipulation. To extend this finding beyond the ear infection model, we confirmed the influence of Hla on neutrophil influx following *S. aureus* infection in another commonly used infection site, i.e. the back skin (Suppl. Fig. 1e). Moreover, treatment of mice with Hla anti-serum augmented neutrophil influx following infection with the clinical isolate USA300, which is the dominant strain causing skin infections in the United States, and which produces high levels of Hla[16] (Suppl. Fig. 1f), suggesting that the neutrophil recruitment defect in the presence of Hla is clinically relevant. Finally, the observed decrease in neutrophil influx in WT *S. aureus* was mirrored by increased bacterial survival (Fig. 1h). Together, these data indicate that Hla interferes with the presence of neutrophils in the skin following infection, and that these effects occur independently of other *S. aureus*-specific factors.

## Neutrophil homing to *S. aureus* infected skin is reduced in the presence of Hla

We hypothesized that the reduced numbers of neutrophils in WT *S. aureus* infected skin were related to their impaired homing into the dermis. Indeed, short-term homing of CFSE-labeled bone marrow cells revealed significantly increased accumulation of neutrophils in ΔHla as compared to WT *S. aureus* infected skin (Fig. 2a). To obtain insight into the mechanism underlying this phenomenon, we performed intravital multi-photon microscopy of infected ears following adoptive transfer of bone marrow cells ($2\times10^7$) from LysM$^{\text{gfp/+}}$

mice[23] (Fig. 2b; Suppl. Movie 1 and data not shown). Donor neutrophil rolling fractions were identical in WT and ΔHla *S. aureus* infected skin (Fig. 2c), indicating that the integrity of the venular endothelium was maintained under both conditions. Similarly, no difference was found in rolling velocities, demonstrating that the expression of adhesion molecules on endothelial cells were the same (Fig. 2d). In contrast, neutrophil sticking fractions were markedly reduced during WT *S. aureus* infection (Fig. 2e), and of those cells that managed to adhere, significantly fewer cells extravasated in response to WT *S. aureus* infection during the imaging period (Fig. 2f, Suppl. Movie 1, **time frame 5:30–7:20 min**). Confocal imaging of infected tissue 1h post adoptive transfer of LysM-EGFP bone marrow cells revealed a large number of GFP+ neutrophils to be present in the interstitium of ΔHla *S. aureus*-infected ear skin, with only a few cells present in WT *S. aureus*-infected tissue (Suppl. Fig. 2a). Flow cytometric analysis of ΔHla *S. aureus* infected tissue confirmed that the vast majority (97.3%) of GFP+ cells were Ly6G+Ly6C^{int} neutrophils. Only 0.8% GFP+ cells represented Ly6G−Ly6C^{hi} monocytes (Suppl. Fig. 2b). Together, these data suggest a major defect in the capability of neutrophil transmigration in WT *S. aureus* infected skin.

Since the conversion of rolling to firm adherence requires chemokine-mediated integrin activation[5, 24], we assessed the production of proinflammatory mediators and chemokines in infected skin. mRNA and protein levels of CXCL1 (KC) and CXCL2 (MIP2), the major chemokines implicated in neutrophil homing, were reduced during WT *S. aureus* infection compared to ΔHla *S. aureus* infection (Fig. 2g and h), as were CCL2 (MCP-1), CCL3 (MIP-1α) and CCL4 (MIP-1β) (Suppl. Fig. 2c). These data suggested that critical neutrophil chemoattractants were reduced in WT *S. aureus*-infected skin.

## PVM can be identified in transgenic DPE-GFP mice, expressing a reporter gene under the control of CD4 regulatory elements

Close inspection of our movie sequences revealed that neutrophils often adhered in small clusters within postcapillary venules (Fig. 2b; Suppl. Movie 2), consistent with recent studies showing the extravasation of neutrophils at distinct "hotspots"[8, 25], although the underlying mechanism for this preferential adherence of neutrophils is unclear. It is conceivable that microenvironmental cues, for example cells located in close proximity to post-capillary venules, may influence neutrophil adherence and extravasation. Based on the fact that CXCL1 and CXCL2, proinflammatory mediators that are preferentially produced by macrophages, were reduced in WT *S. aureus* infected skin, and that macrophages are often found in close proximity to blood vessels, we further tested the involvement of macrophages in neutrophil recruitment. In order to do so, we made use of transgenic DPE-GFP mice, in which GFP is expressed under the control of the CD4 enhancer/promoter[26]. While αβ T cells are uniformly GFP+ in these mice, we have recently discovered that a specific subset of cutaneous macrophages, namely PVM, also express GFP at higher levels than T cells (Fig. 3a and b). Thus, GFP+ cells with an elongated, dendritic shape were found to localize directly adjacent to post-capillary venules within the skin of DPE-GFP mice. On average, 38±3% (mean±SEM) of the length of venules were associated with PVM (Fig. 3a; Suppl. Movie 3). Flow cytometric analysis revealed that these GFP^{hi} cells were CD45+CD3−CD326−CD11b^{hi}F4/80+ (Fig. 3b). They also exhibited high cell surface expression of the resident tissue macrophage markers CD64 and ATP binding cassette

transporter A1 (Suppl. Fig 3a). Based on these anatomical and phenotypic characteristics, we inferred that GFP expression in the skin of DPE-GFP mice identified PVM. A second macrophage population that exhibited lower expression of *Cd4* mRNA and did not express GFP was further identified in the skin of DPE-GFP mice (Fig. 3c and d), and expressed comparable surface markers as PVM (Fig. 3d and Suppl. Fig. 3a).

GFP[+] macrophages were also observed in association with post-capillary venules in the cremaster muscle of DPE-GFP mice (Fig. 3e), consistent with the previous description of "adventitial" macrophages[9]. These cells were in close association with pericytes and did not directly contact endothelial cells (Suppl. Fig. 3b). In contrast, microglia, Langerhans cells, Kupffer cells and alveolar macrophages were GFP[−] (data not shown). Transcriptional profiling of GFP[+]F4/80^{+} skin cells revealed expression of *Csf1r*, which encodes the CSF-1 receptor and is essential for macrophage development and homeostasis (Suppl. Fig. 3c)[27]. Further transcriptional comparison between GFP[+] vs GFP[−] macrophages from DPE-GFP mice revealed a small but significant increase in *Tlr4* expression by PVM, while both subpopulations expressed comparable levels of mRNA for other common macrophage proteins (Suppl. Fig. 3d).

PVM could also be identified in *Csf1r*-EGFP (MacGreen) mice[28] (Suppl. Fig. 3e). The vascular association of blood vessels with PVM in MacGreen mice was determined at 40±6%, similar to DPE-GFP mice. Since the vast majority of F4/80[+] macrophages (>95%) in the skin of MacGreen mice are GFP[+] (data not shown), these data suggest that GFP expression in DPE-GFP mice demarks most, if not all, PVM. We then performed intravital imaging to explore the steady-state behavior of GFP[+] PVM in skin. As shown in Fig. 3f and Suppl. Movie 4, these cells were non-migratory, but displayed continuous movements of their dendrites. Similar behavior has been associated with scanning/sampling of the microenvironment in other leukocyte populations, particularly dendritic cells[29].

### PVM interact with blood-borne neutrophils during extravasation

To test whether PVM were involved in neutrophil recruitment during *S. aureus* infection, we adoptively transferred red fluorescent protein (RFP)-expressing bone marrow cells from mT/mG mice[30] into ΔHla *S. aureus*-infected DPE-GFP mice and analyzed their adherence to and extravasation from dermal venules by intravital multi-photon microscopy (93.4% ± 2.1% of transferred cells that extravasated into infected skin were neutrophils; data not shown). Neutrophils that crawled along the endothelium appeared to be attracted towards GFP[+] PVM (Fig. 4a; Suppl. Movie 5). 82±4% of neutrophils that adhered in post capillary venules did so within 0–20 μm of PVM localization. 83% of neutrophil extravasation hotspots co-localized with PVM, and 80% of neutrophils exited venules within 0–20 μm of PVM. Since PVM associated with 38±3% of the wall of dermal venules, we further evaluated whether this neutrophil-macrophage correlation differed from that expected from chance alone by randomizing neutrophil extravasation throughout the entire lengths of analyzed post-capillary venules (Suppl. Fig. 4a; see Materials and Methods section for detailed description). Indeed, this analysis confirmed a preferential bias of neutrophil extravasation towards regions proximal to perivascular macrophages (Fig. 4b). A similar correlation between neutrophil extravasation and PVM localization was observed following

intradermal injection of *E. coli* (Suppl. Fig. 4b and c), indicating that this phenomenon was not unique to *S. aureus* infection. Moreover, concomitant injection of *E. coli* with purified *S. aureus* hemolysin resulted in reduced neutrophil influx, ear thickness and RBC counts (Suppl. Fig. 4d–f), similar to those observed for WT *S. aureus* infection.

Based on these observations, we tested the production of chemokines by GFP⁺ PVM. To this end, PVM and, for comparison, GFP⁻ macrophages, dermal dendritic cells, dermal γδ T cells and keratinocytes were isolated from the skin at six hours after ΔHla *S. aureus* infection and sorted to high purity. Quantitative RT-PCR revealed that GFP⁺ PVM were the prime producers of *Cxcl1, Cxcl2, Ccl2, Ccl3*, and *Ccl4* (Fig. 4c and Suppl. Fig. 5). In contrast, GFP⁻ macrophages expressed significantly lower levels of all tested chemokines but significantly higher amounts of *Il-1β*, while non-macrophage populations were negative for most chemokines, with the exception of low amounts of *Cxcl1* in γδ T cells and keratinocytes.

Together, these data indicate that GFP⁺ PVMs are a major source of chemokines that have been implicated in neutrophil attraction and guide neutrophils during extravasation into infected dermis.

## Hla induces rapid lysis of macrophages *in vitro*

Since both neutrophil sticking on the endothelium as well as extravasation were impaired in WT *S. aureus* infection as compared to the Hla-deficient strain, we hypothesized that macrophages may be sensitive to Hla-induced toxicity. To explore this possibility further, we exposed leukocytes harvested from the peritoneal cavity or peripheral blood to Hla *in vitro* (Fig. 5a). Monocytes and macrophages were exquisitely sensitive to Hla, while neutrophils, dendritic cells and B cells resisted Hla-induced lysis, which occurred in a time and concentration dependent manner (Fig. 5b). Real time imaging indicated a rapid loss of membrane integrity in macrophages during the early phase, thereby confirming lytic cell death (Fig. 5c; Suppl. Movie 6 and data not shown). Lysis was also observed for GFP⁺ macrophages harvested from ear skin (Fig. 5d).

To determine the mechanisms underlying the specificity of Hla-induced cell death, we then measured the expression of ADAM10, which has been implicated in Hla binding to cells[19, 21]. While neutrophils, dendritic cells and B cells were low for ADAM10 expression, macrophages, including GFP⁺ dermal PVM, expressed high levels (Fig. 5e–g; Suppl. Fig. 6). Furthermore, pretreatment of peritoneal macrophages with the ADAM10-specific inhibitor GI254023X[31] significantly reduced Hla-mediated lysis (Fig. 5h). Together, these data provide a molecular basis for the preferential macrophage killing by Hla.

## Hla induces rapid lysis of GFP⁺ PVM *in vivo*

Finally, we set out to determine whether *S. aureus*-derived Hla impacted on PVM integrity *in vivo*. In order to visualize injected bacteria *in vivo*, we engineered both WT and ΔHla *S. aureus* to express red fluorescent protein (RFP), which did not affect the growth of *S. aureus* strains *in vitro* or neutrophil influx into the skin *in vivo* (data not shown). On initial contact with bacteria, PVM rapidly phagocytosed both WT and ΔHla *S. aureus* (Fig. 6a; Suppl.

Movies 7&8). However, GFP⁺ PVM around WT *S. aureus* injection sites rapidly retracted their dendrites, which was followed by their sudden disappearance within 2h of injection (Suppl. Movies 7&9), consistent with the lytic cell death observed *in vitro* (Fig. 5a–d). In contrast, GFP⁺ PVM remained intact following injection of inert beads (Fig. 6b&c; Suppl. Movie 10). Importantly, ΔHla *S. aureus* induced only occasional PVM death (Fig. 6b and c; Suppl. Movie 11), indicating that their destruction by WT *S. aureus* was Hla-dependent. Furthermore, viability of dermal dendritic cells in CD11c-YFP mice[32], γδ T cells and ILC2 cells in *Cxcr6*⁺/gfp mice[33, 34], and keratinocytes in mT/mG mice[30] *in situ* was not impacted by WT *S. aureus* (Fig. 6b&c; Suppl. Movies 12&13 and data not shown). Consistently, freshly isolated keratinocytes did not express ADAM10, and we did not observe evidence for the killing of these cells by Hla *in vitro* (data not shown). Furthermore, vascular integrity, as shown by staining for CD31 and laminin was not affected by WT *S. aureus* even 6h post infection (Suppl. Fig. 7a), indicating that endothelial cells were not susceptible to Hla-induced lysis during early *S. aureus* infection. This was corroborated by the fact that vascular leakage (measured by Evans Blue extravasation) was much more pronounced post ΔHla *S. aureus* as compared to WT *S. aureus* infection (Suppl. Fig. 7b and Suppl. Movie 1, timepoint 03:00 onwards). Finally, anti-Thy-1 staining on whole mount dermal specimens did not provide evidence for damage of Thy-1 expressing stromal cells 6 hr post WT *S. aureus* infection (Suppl. Fig. 7c). Taken together, these data indicated that macrophages and not other stromal components or epithelial cells are the prime target of Hla during the early phase of intradermal *S. aureus* infection *in vivo*.

Twelve hours following challenge with RFP-expressing *S. aureus*, the absolute numbers of RFP⁺ neutrophils were significantly reduced in mice infected with WT *S. aureus* when compared to ΔHla *S. aureus* (Fig. 6d), consistent with their reduced recruitment. However, the percentage of neutrophils that had internalized bacteria did not differ between tissues infected with WT and ΔHla *S. aureus* (Suppl. Fig. 8a). Moreover, mean fluorescence intensities of RFP-expressing *S. aureus* strains were comparable, as were the intensities of RFP⁺ neutrophils (Suppl. Figs 8b and 8c), indicating that similar numbers of bacteria were taken up by neutrophils on an individual cell basis. We concluded that Hla did not directly influence the uptake of bacteria by neutrophils, and that the increased bacterial burden in WT *S. aureus* compared to ΔHla *S. aureus* infected tissue was therefore primarily due to the reduced number of neutrophils recruited to the site. Thus, PVM-mediated regulation of neutrophil recruitment in infected skin is a critical determinant of bacterial survival and tissue reconstitution during *S. aureus* infection.

## Discussion

Neutrophil extravasation is a tightly controlled process that is thought to primarily depend on molecular cues displayed on post-capillary endothelial cells. Thus, a cascade of consecutive interactions occurring between blood-borne neutrophils and the endothelium, characterized by rolling, firm adhesion and transendothelial migration, ensures the timely arrival of neutrophils at sites of inflammation. Our data reveal that PVM, a thus far unrecognized player in this process, provide via chemoattractant production biochemical guidance of neutrophils into the cutaneous interstitial space. Furthermore, our data indicate that *S. aureus*, a pathogen that usually enters the body via the skin, directly impedes

neutrophil extravasation via Hla-dependent destruction of PVM. The fact that *S. aureus* exploits this pathway highlights its importance in the innate immune defence against bacterial pathogens.

While the central features of leukocyte recruitment into inflamed tissues have been validated in many experimental models[1, 3], recent findings have also implied a role for tissue resident cells that associate with blood vessels in the coordination of inflammation. Venular pericytes, which lie between endothelial cells and the basement membrane (BM) and ensheath the vessel itself, have been shown to support neutrophil crawling during their egress from the vessel lumen[8]. Furthermore, NG2-expressing arteriolar and capillary pericytes activate and guide neutrophils after their extravasation and support their interstitial migration via provision of macrophage migration inhibitory factor[35]. Our data support a scenario where extravascular PVM directly impact on the adhesive and transmigratory activity of neutrophils in the blood stream. Thus, intraluminally crawling neutrophils finally extravasate, in the majority of cases (80%), in areas juxtaposed to GFP[+] PVM. In the absence of PVM, firm adherence and TEM are markedly reduced. While we do not have evidence that PVM processes directly reach into the lumen of dermal venules, they associate tightly with pericytes, indicating that they may assist or mediate the previously observed crawling of neutrophils between pericytes. Mechanistically, based on their expression of *Cxcl1* and *Cxcl2* mRNA, PVM appear to create an appropriate chemokine milieu for the egressing neutrophil. The discontinuous association of PVM with the vessel wall implies the existence of confined areas of increased chemokine deposition within post-capillary venules and subsequent patchy arrest of neutrophils. Consistently, we noted that following challenge with ΔHla *S. aureus*, neutrophils arrested in small clusters, rather than continuously along the venular wall, and preferentially extravasated at circumscribed locations that were adjacent to PVM. Neutrophil extravasation hotspots have been reported to occur due to a range of mechanisms including the presence of tricellular junctions[36], pericyte gaps[8], or to regions of low basement membrane protein expression[37]. Collectively, based on their intimate association with the vessel wall, PVM are thus in an ideal position to contribute to focal chemokine gradients, which may either be transported to the luminal surface of endothelial cells and/or act as a migratory cue directly after TEM.

Although the existence of PVM within the dermis has been sporadically reported, this has generally been an incidental finding, and no particular functions have been ascribed to them[9, 38]. Given the striking capacity of DPE-GFP[+] PVM to produce chemokines and mediate neutrophil recruitment, this raises the question of whether analogous populations exist in other organs. Preliminary analysis of GFP-expressing perivascular cells in a range of tissues of DPE-EGFP mice, including cremaster muscle, meninges and adipose, indicated the presence of such cells. However, in other organs, such as the lungs and spleen, GFP[+] PVM were scarce or absent. These findings may help explain some of the well-documented organ-specific differences in leukocyte homing during inflammation. Skin and muscle, for example, display, by and large, similar molecular requirements for neutrophil entry, while in the lungs and spleen leukocyte homing follows different rules.

Another salient observation from DPE-GFP mice was the existence of macrophage heterogeneity within the dermis, as indicated by the presence of GFP[+] and GFP[−]

populations. While the phenotypic profile of these cells was largely identical (with the exception of *Cd4* and *Tlr4* mRNA expression), they exhibited distinct functional properties, as demonstrated for chemokine and cytokine production profiles. Macrophage heterogeneity within a single tissue, in terms of both developmental pathways and functions, has previously been reported. For example, in the brain, a numerically major population comprises long lived and/or self-renewing microglia, which originate from yolk-sac derived precursors during embryogenesis[39]; however, the existence of a second population of perivascular macrophages that originate from hematopoietic sources has long been appreciated.[10] Future studies will have to determine the precise lineage relationship of GFP[+] and GFP[−] dermal macrophages during ontogeny and in adult animals.

While bacterial virulence factors have been studied extensively in the past, how exactly they disrupt specific microenvironments is poorly understood. To the best of our knowledge, our study provides the first direct visualization of the action of a defined virulence factor, Hla, in real time *in situ*. Although the virulence of *S. aureus* certainly cannot be ascribed to any single factor, it is accepted that Hla, which shows near ubiquitous expression by clinical isolates, is a major determinant. We observed diminished adhesion of neutrophils during WT *S. aureus* infection, which is in line with the previously described reduced leukocyte homing induced by *E. coli* expressing alpha-hemolysin[40]. The main finding of our live microscopy experiments was the rapid and specific destruction of GFP[+] PVM by Hla. The resultant impact on neutrophil homing into inflamed skin is consistent with several different strategies employed by *S. aureus* to modulate neutrophil functions[41]. Nevertheless, given the indispensable role of Hla in the induction of tissue necrosis, it is plausible to postulate that Hla-mediated destruction of PVM represents a major mechanism by which the bacterium thwarts the ensuing innate immune response, at least during its earliest phase. During later stages, other bacterial factors, such as PSMs and other leukocidins, which exhibit neutrophil chemotactic activity and are primarily produced by CA-MRSA, may also play a role[16]. Indeed, neutrophils continue to be recruited even in wildtype *S. aureus* infections, albeit at reduced numbers as compared to Hla-deficient bacteria. Collectively, our findings thus argue that the net effect of Hla-mediated PVM destruction is a delay in neutrophil influx into the dermis, which is thereby likely to give the bacterium a survival advantage.

The specificity of macrophage killing by Hla likely relates to the high expression of its receptor ADAM10 on macrophages. Mechanistically, binding of Hla to ADAM10 in epithelial cells during lung inflammation was demonstrated to induce ADAM10 activity, which eventually mediates the breakdown of epithelial integrity via cleavage of E-cadherin[19]. Such a pathway was proposed to be the dominant cause of necrosis in both pulmonary[19] and cutaneous[20] infection models. Other studies have suggested that Hla acts predominantly as a cytotoxin[21, 42], and our data are consistent with this notion, since Hla lysed macrophages from various sources both *in vitro* and *in vivo*. Nevertheless, our data do not discount the reported role for Hla/ADAM10 interactions in mediating virulence through disruption of epithelial integrity. In our model we observed tissue necrosis at times beyond 24 hours p.i. but cannot formally ascribe this to increased bacterial load. This finding is consistent with recent studies by Inoshima *et al.* who specifically targeted ADAM10 deletion to keratinocytes[20] or alveolar epithelial cells[19]. Following WT *S. aureus* infection,

these authors found that necrosis occurred at later stages of infection but this was not associated with changes in bacterial numbers, which suggests that independent mechanisms may underpin necrosis and bacterial clearance.

PVM in human skin may contribute in a similar manner to neutrophil recruitment during bacterial infection, and may also be targets of *S. aureus*. Thus, the interference with Hla-ADAM10 interactions on these cells by small molecule inhibitors or anti-Hla antibodies may prove a useful treatment strategy for antibiotic-resistant *S. aureus* infections.

In summary, we have described a population of PVM that is a dominant source of neutrophil-recruiting chemokines during dermal *S. aureus* infection. The existence and likely functions of PVM emphasize the critical role of non-endothelial, but blood vessel associated cells in the co-ordination of leukocyte extravasation. The selective killing of PVM by *S. aureus* produced Hla results in diminished availability of chemokines immediately following bacterial invasion. This is likely to give the bacterium an extended window of opportunity to proliferate in the absence of antimicrobial neutrophil effector mechanisms. Thus, the fine-tuning of the inflammatory influx by skin resident cells during the first hours of bacterial invasion is critical for the control of infection.

## Materials and Methods

### Mice

C57BL/6 (WT) mice were purchased from the Animal Resources Centre (Perth, Australia). Albino C57BL/6 (C57BL/6-Tyrc-2J also referred to as WB6) and mT/mG mice[30] were purchased from The Jackson Laboratory; LysM-EGFP mice were a kind gift from Thomas Graf[23] Csf1r-EGFP (MacGreen) mice were a kind gift from David Hume[28]. CD11c-YFP mice[32] were a kind gift from Michel Nussenzweig. DPE-GFP mice were described previously[26]. Mice were bred and maintained on the C57BL/6 background in pathogen–free conditions at the Centenary Institute animal facility. 8–16 week old mice of either sex were used for experimentations. The Animal Ethics Committee of University of Sydney approved all animal experiments.

### Bacterial strains

*S. aureus* 8325-4 (WT) and its isogenic Hla-deficient strain *S. aureus* DU1090 (ΔHla) were kindly provided by Dr. Mark Willcox, University of NSW, Australia. *S. aureus* DU1090 was generated as described previously[43]. *S. epidermidis* ATCC12283 and *E. coli* DH5α (Invitrogen) were used as indicated. USA300 was a kind gift from Dr. Elizabeth Harry, University of Technology Sydney. Bacteria were grown to mid log-phase in Luria-Bertani (LB) broth, washed, and resuspended in PBS. Bacterial concentrations were estimated with a spectrophotometer by determining the optical density at 600 nm ($OD_{600}$). Colony-forming units (CFUs) were verified by plating dilutions of the inoculum onto LB agar overnight at 37°C.

### Generation of red fluorescent protein (RFP)-expressing S. aureus strains

The shuttle-plasmid pSK9054 was used in order to express RFP in *S. aureus* strains. On pSK9054, the moderate-strength staphylococcal promoter, $P_{orf90}$, was used to drive the transcription of mRFPmars[44], a fluorescent protein that is highly codon-adapted to *S. aureus*. Transcription from the $P_{orf90}$ promoter in pSK9054 is constitutive, and *S. aureus* cells expressing mRFPmars from this plasmid attain a high-level of fluorescence (Suppl. Fig. 8c). A DNA fragment containing the mRFPmars ORF, which included a strong ribosomal binding site upstream from the initiation codon, was amplified by PCR from plasmid pmRFPmars[44] (Addgene plasmid 26252) with sense oligonucleotide AB62 (CGGGATCCTAGGAAAGGAGGATG) and anti-sense oligonucleotide AB63 (GGGGTACCTTAATGATGGTGGTGATGATGG), using iProof™ High Fidelity DNA Polymerase (Bio-Rad). Following amplification, the resultant 727 bp fragment was purified using a Bioline ISOLATE PCR and Gel Kit, prior to digestion with KpnI restriction endonuclease (NEB). The digested fragment was purified as per above, and was treated with T4 polynucleotide kinase (PNK; NEB) in order to phosphorylate the blunt 5′ end of the amplicon. Concurrent with this process, 2 μg of plasmid pSK7063[45] DNA was digested with BamHI (NEB), gel purified (Bioline ISOLATE PCR and Gel Kit), and the recessed ends of the digested fragments were in-filled using Pfu DNA polymerase (Stratagene). The blunted plasmid fragment was purified as above, prior to digestion with KpnI. pSK7063 DNA prepared in this way was used in a ligation reaction with the amplified mRFPmars ORF fragment, and then used to transform chemically competent *E. coli* DH5α cells. The integrity of a resulting construct was checked by sequencing (Australian Genome Research Facility) and designated pSK9054. RFP-expressing derivatives of *S. aureus* strains 8325-4 and DU1090 were obtained by electroporation of pSK9054 essentially as described previously[46].

### Mouse model of cutaneous bacterial infection and in vivo blocking of Hla

Approximately $10^7$ CFUs of bacteria were injected intradermally in a small volume of PBS (4μl) into the pinnae of each ear using a 29g insulin syringe (BD). In some experiments, bacteria ($10^7$ CFUs) were injected subcutaneously into the back skin of mice. In some experiments, injections of ΔHla *S. aureus* were combined with Hla purified from *S. aureus* (Sigma-Aldrich). For *in vivo* blocking of Hla, 8h before infection mice were administered intra-peritoneally with 2.5mg of whole antiserum against Hla or control rabbit serum (both from Sigma-Aldrich). Sera were dialysed in PBS before use. For intravital imaging, approximately $2\times10^6$ CFUs of bacteria were injected into the pinnae of each ear in a volume of 0.5μl PBS using a 35g Hamilton syringe.

### Tissue processing and flow cytometry

Isolation of skin cells involved the following process: Ears were split into dorsal and ventral halves using forceps and subjected to enzymatic digestion with collagenase type IV (2 mg/ml, Sigma-Aldrich) in PBS for 60 min at 37°C to release cells. To obtain single-cell suspensions, the tissues were filtered through an 80μm stainless steel mesh. Cell and RBC numbers were determined using a hemocytometer. For flow cytometric analysis, single-cell suspensions were incubated with anti-CD16/32 (2.4G2; BD) to block Fc receptors and

stained with fluorochrome-conjugated antibodies diluted in "FACS buffer" (PBS containing 5% FCS, 2 mM EDTA, and 0.02% sodium azide). Resident tissue macrophages from spleen and peritoneal cavity were isolated and identified as descried previously[47]. Fluorochrome-conjugated antibodies (purchased from BD, eBioscience, BioLegend, AbD Serotec, R & D Systems or Invitrogen) against the following cell surface molecules were used: CD45 (clone 30-F11), CD11b (clone M1/70), Ly6G (clone 1A8), Ly6C (clone HK1.4), CD64 (clone X54-5/7.1.1), F4/80 (clones BM8 or Cl:A3-1), ABCA1 (clone 5A1-1422), CD36 (clone HM36), CD169 (clone MOMA1), ADAM10 (clone 139712), CD326 (clone G8.8), CD19 (clone 1D3), CD3 (clone 145-2C11), NK1.1 (clone PK136) CD68 (clone FA-11). Samples were first stained for cell surface molecules and aquafluorescent reactive dye (Invitrogen) for dead cell exclusion after fixation with 4% formalin. In some experiments cells were analyzed unfixed and DAPI was used as a viability marker. Samples were acquired on a LSR Fortessa or 10-laser LSR SORP flow cytometer (BD) and data were analyzed using FlowJo software (Tree Star, Inc.). Sorting was performed using a 10-laser Influx sorter (BD).

### Whole mount staining

Whole mount staining on infected ears was performed as described previously[33]. Briefly, dorsal and ventral halves of untreated or WT *S. aureus* infected ears were split 6 hour p.i. The dorsal halves were fixed in 4% paraformaldehyde for 30 min at 37°C. The tissue was washed with PBS containing 5% FCS, 0.3% Triton X100 and 2mM EDTA (immunostaining buffer) for 30 min at 37°C. The samples were then incubated with anti-CD31 (Clone:MEC13.3, BD biosciences) and anti-laminin (Sigma-Aldrich) primary antibodies overnight at 4°C. The tissue samples were washed three times with immunostaining buffer and incubated with Goat Anti Rat Alexa 647 and Goat Anti Rabbit Alexa 405 antibodies for 4 hr at 4°C. The tissues were thoroughly washed and mounted using antifade (DABCO). For Thy-1 staining anti-Thy-1 (Clone: 30-H12, BD biosciences) primary antibody was used followed by goat anti rat Alexa 647 as the secondary antibody. For imaging of cremaster muscle, the tissue was exteriorized, dissected, fixed in 4% paraformaldehyde for 30 min at 37°C and processed as described above. The tissue was then stained with anti-CD31 (Clone:MEC13.3, BD biosciences) and anti-smooth muscle actin (Clone: 1A4, Abcam) followed by goat anti rat Alexa 647 and goat anti rabbit Alexa 594 antibodies. Confocal imaging was performed using Leica TCS SP5 confocal microscope system. Images were processed using Volocity software (Perkin Elmer).

### Quantification of tissue bacterial burden after infection

*S. aureus* strains (WT and ΔHla) were inoculated intradermally into the ears as described above. At 24, 48 and 72 hours p.i., ears were harvested, weighed and then mechanically homogenized using a rotor stator homogeniser (Polytron, Lucerne, CH) in 2 mL of sterile PBS. Serial dilutions of ear homogenates were plated on LB agar plates. Plates were incubated at 37°C overnight and CFUs were counted the following day.

## Histologic analysis of skin lesions

Pinnae of PBS or *S. aureus* infected mice were fixed in 10% neutral buffered formalin and hematoxylin and eosin sections prepared according to standard procedures.

## Cytokine measurement of tissues

Cytokine and chemokine content of tissue homogenate was measured using Cytometric Bead Array assay (BD) as recommended by the manufacturer. CXCL2 protein in homogenates was quantified using a Quantikine ELISA kit (R & D Systems). Briefly, tissues were mechanically homogenized using a rotor stator homogeniser (Polytron) in PBS containing protease inhibitors (Halt™ protease inhibitor; Thermo Scientific) and 5mM EDTA. The homogenate was then centrifuged 15,000g for 10 min at 4°C. The resulting supernatant was then used for cytokine quantification.

## RT-qPCR

Tissues were homogenized in RLT buffer (Qiagen, CA), using a rotor stator homogeniser (Polytron). RNA was extracted using an RNeasy miniprep kit (Qiagen) following the manufacturer's instructions and reverse-transcribed using Moloney murine leukemia virus-RT (Ambion) primed with random hexamers (GeneWorks, Australia). Quantitative PCR was performed using the primers listed below on a Corbett Research Rotor Gene 3000 using kapa SYBR Green (KAPA Bioystems, MA) with cycling conditions as follows: 2 min 95°C denaturation and then 35 repeats of a two-step amplification cycle (95°C for 15s and 60°C for 45s). Following amplification, product purity was assessed by melt-curve analysis. Gene-expression levels were normalized against the geometric mean of 4 reference genes (HPRT, RPL13a, β-actin and YWHAZ). In tissue samples, expression was then normalised to the PBS challenged group. The following primers were used for RT-qPCR: RPL13a: RPL13a: 5′-CTTAGGCACTGCTCCTGTGGAT-3′ (sense) and 5′-GGTGCGCTGTCAGCTCTCTAAT-3′ (antisense); HPRT: 5′-GCTTTCCCTGGTTAAGCAGTACA-3′ (sense) and 5′-CAAACTTGTCTGGAATTTCAAATC-3′ (antisense); YWHAZ: 5′-TGTCACCAACCATTCCAACTTG-3′ (sense) and 5′-ACACTGAGTGGAGCCAGAAAGA-3′ (antisense); β-actin: 5′-CCCCAACTTGATGTATGAAGGC-3′ (sense) and 5′-TCAAGTCAGTGTACAGGCCAGC-3′ (antisense); CXCL1: 5′-TGTCAGTGCCTGCAGACCAT-3′ (sense) and 5′-CCTGAGGGCAACACCTTCA-3′ (antisense); CXCL2: 5′-CCCTCAACGGAAGAACCAAA-3′ (sense) and 5′-AGGCACATCAGGTACGATCCA-3′ (antisense); IL-1b 5′-GTGGTTCGAGGCCTAATAGGCT-3′ and 5′-AGCTGCTTCAGACACCTTGCA- 3′ (antisense); (sense), CCL2: 5′-GGCTCAGCCAGATGCAGTTAA-3′ (sense) and 5′-CCTACTCATTGGGATCATCTTGCT-3′ (antisense); CCL3: 5′-CATATGGAGCTGACACCCCG-3′ (sense) and 5′-CGTGGAATCTTCCGGCTGTA-3′ (antisense); CCL4: 5′-AGGGTTCTCAGCACCAATGG-3′ (sense) and 5′-GCTGCCGGGAGGTGTAAGA-3′; F4/80: 5′-GGCATACCTGTTCACCATTATCAAC-3′ (sense) and 5′-CCTGGTGAGGAGTTTCTTATATTCATC-3′ (antisense); γδTCR: 5′-TTTGAACCATATGCAAATTCTTTCA -3′ (sense) and 5′-

GTGACTCTTGGGCCATAGCAA-3′ (antisense); MHC class II: 5′-AGTCACACCCTGGAAAGGAAGG-3′ (sense) and 5′-TCACCCAGCACACCACTTCTT-3′

## Quantification of gene expression in sorted macrophages

Briefly, ears were injected with live ΔHla *S. aureus,* and 4–6 hours later cell suspensions were prepared and stained for flow cytometric analysis. Cell populations were identified as follows: macrophages (DAPI⁻CD45⁺CD11b^hiCD64^hi), dendritic cells (DAPI⁻CD45⁺CD64⁻MHCII^hi), γδT cells (DAPI⁻CD45⁺CD64⁻MHCII⁻CD3⁺ γδT⁺) and keratinocytes (DAPI⁻CD45⁻CD326⁺CD90⁻). Cells were sorted (1000–2000 per population depending on experiment) using an Influx sorter (BD) into RLT plus lysis buffer (Qiagen). Due to low numbers of cells isolated from ears, sort purity was assessed by expression of cell population specific genes (Suppl Fig 5). RNA was extracted using an RNeasy micro plus kit (Qiagen), followed by RT-qPCR as described for tissue homogenates.

## Homing experiments

Mice were infected with *S. aureus* (WT or ΔHla) for 10h as described above. Afterwards, $10^7$ CFSE-labeled bone marrow cells were adoptively transferred via tail vein injection. Two hours later, ears were harvested and quantified for the presence of CFSE⁺Ly6G⁺ neutrophils. For confocal imaging, mice were infected for 6h with labeled WT or ΔHla *S. aureus* following which $10–20\times10^6$ LysM-EGFP bone marrow cells were adoptively transferred and tissue harvested 1h post transfer. Tissue samples were stained and imaged as described above or harvested for flow cytometry.

## Myeloperoxidase assay

Samples were homogenized in potassium phosphate buffer (pH 6.0) containing 0.5% hexadecyltrimethylammonium bromide. The suspension was centrifuged at 18,000g for 20 min, and 10μl of supernatant was added to 190μl of potassium phosphate buffer (pH 6.0) containing 0.167 mg/ml o-dianisidine dihydrochloride (Sigma) and 0.0005% hydrogen peroxide. Activity of MPO in tissues was determined by absorbance at 460nm.

## Multi-photon intravital imaging of skin and image analysis

Preparation of animals and imaging was performed as previously described[22]. In brief, mice were anesthetized by i.p. injection of Ketamine/Xylazine (80/10mg/kg), with repeated half-dose injections as required. The ears were treated with Nair cream (Church & Dwight) to remove hairs. The animals were then placed onto a custom-built stage to position the ear on a small metal platform for multi-photon (MP) imaging. The ear was immersed in PBS/glycerin (70:30, vol:vol) and covered with a coverslip. The temperature of the platform was regulated independently, and maintained at 35°C, whereas the body temperature was kept at 37°C using a heating pad placed underneath the mouse. MPM imaging was performed on a LaVision BioTec TriMScope attached to an Olympus BX-51 fixed stage microscope equipped with 20x (NA 0.95) water immersion objectives. The setup includes six external non-descanned dual-channel reflection/fluorescence detectors, a diode pumped, wideband mode-locked Ti:Sapphire femtosecond laser (MaiTai HP; SpectraPhysics, 720nm–1050nm,

<140fs, 90MHz), and an APE Optical Parametric Oscillator system (tuning range 1050–1400nm). To understand the neutrophil recruitment defect, ears of WB6 mice were injected intradermally with 2–3×10$^6$ CFUs of either WT or ΔHla *S. aureus* bacteria in a volume of 0.5μl PBS using a 35g Hamilton syringe. After 6 hours, ears were mounted onto the imaging stage as described above. Bone marrow cells (10–20×10$^6$) from LysM-EGFP mice were injected intravenously followed by Evans blue (Evans blue conjugated to BSA) and imaging was performed for 300×300 μm region of the ear dermis at 250×250 pixel resolution at 1 frame/second for 10 min. For observing the correlation between neutrophil extravasation and perivascular macrophages in DPE-GFP mice, 2–3×10$^6$ CFUs of ΔHla *S. aureus* bacteria were injected in a volume of 0.5μl PBS 6h before imaging. Bone marrow cells (10–20×10$^6$) from mT/mG mice were injected intravenously followed by Evans blue and imaging was performed for 300×300 μm region at 500×500 pixel with 6–8 z steps 4 μm apart for 20–30 min. In experiments involving perivascular macrophage cell death fluorescent beads, RFP-expressing WT *S. aureus* or ΔHla *S. aureus* bacteria were used for infection and imaging performed immediately. Images were recorded for 500×500 μm region at 500×500 pixel with 10–12 z steps 4 μm apart every 2 min for 2hr. All images were processed using Image J (NIH, Bethesda) and image stacks were then transformed into movies using Volocity software (PerkinElmer). Migration parameters and cellular interactions were determined using Volocity as described previously[48].

### Analysis of intravascular neutrophil behaviour

Neutrophil rolling was defined as the movement of cells along the blood vessel wall at a velocity lower than free flowing cells. Sticking was defined as neutrophil arrest for more than 30s without movement of more than one cell diameter. Extravasation was defined as the migration of sticking cells from the vessel lumen to the interstitium during the period of analysis. Only post-capillary venules were considered and the complete observation period (at least 10 min) of data acquisition was analyzed.

$$\text{Rolling fraction} = \text{Number of cells rolling in blood vessels}/\text{total number of cells observed}$$
$$\text{Rolling velocity} = \text{Distance travelled by the cells in blood vessel lumen } (\mu m)/\text{time (sec)}$$
$$\text{Sticking fraction} = \text{Number of cells sticking in blood vessels}/\text{total number of cells observed}$$
$$\text{Sticking to extravasation conversion} = \text{Number of cells extravasating from blood vessels}/\text{Number of cells sticking in blood vessels}$$
$$\% \text{ Loss of perivascular macrophages} = (\text{Number of GFP+cells at end of imaging}/\text{ Number of GFP+cells at start of imaging}) \times 100$$

### Determination of vascular association of blood vessel to PVM

Vascular association refers to the length of blood vessel associated with PVMs and was calculated using the following formula:

$$\% \text{ Vascular association} = [\text{cumulative length of PVMs along blood vessel wall } (\mu m)/\text{total length of blood vessel } (\mu m)] \times 100$$

To determine this fraction for *Csf1r*-EGFP (MacGreen) mice, intravital imaging was performed for up to 2hrs and only non-migratory GFP$^+$ cells along blood vessels were considered for analysis.

## Methodology to determine neutrophil-perivascular macrophage interactions

The total events of neutrophil extravasation observed experimentally were arranged at equal distance to one another in the blood vessel under analysis (each blood vessel for each set of observation). The proximity of these equally distributed simulated extravasation locations to the nearest PVM was measured and used as the predicted measurement (Suppl. Fig. 4a). In both cases of observed and predicted values only the perivascular macrophage on the same side of the neutrophil extravasation were considered. "Hotspots" were defined as regions along the blood vessels from where 2 or more neutrophils extravasated during the imaging period.

## Quantification of cell lysis in situ

Image stacks (500×500 μm, 10–12 z planes at 4μm step size) were recorded every 2 min for 2hr. Indicated fluorescent cells were counted at the start and end time points. Cell death was calculated as % viable cells at the end if the imaging session.

## Hla treatment in vitro

Whole blood from WT C57BL/6 mice was collected in Alsevers solution prior to RBC lysis in ACK Lysing Buffer (Life Technologies) and washing in serum-free RPMI (Life Technologies) prior resuspension in RPMI and Hla treatment (7.5μg/ml) at 37°C for 3 hours. Peritoneal lavages from WT C57BL/6 mice were collected and pooled in serum-free RPMI before separating into 400μl aliquots at a concentration of $10^6$ cells/ml. Hla was added at indicated concentrations and incubated up to 4 hours in RPMI at 37°C. For inhibition of ADAM-10 dependent Hla-mediated lysis, peritoneal cells were pre-incubated with 80μM GI254023X (Okeanos Tech.) for 60min at 37°C followed by addition of a two-fold stock Hla leading to a final concentration of 40μM GI254023X[49] and 10μg/ml of Hla in the cell suspension which was incubated for a further 20–30 minutes. Following incubation, cells were washed in FACS buffer and stained with anti-CD19 APC-Cy7 or PE (clone 1D3), anti-CD11c PE-Cy7 (clone HL3), anti-CD11b FITC (clone M1/70) and anti-F4/80 PE (clone BM8) or A647 (clone: CI:A3-1) antibodies (all purchased from BD or AbD Serotec) and assessed by flow cytometry using 10-laser LSR II cytometer (BD). Data were analyzed using Flowjo software (Tree Star, Inc.). Live B cells (CD19^{+}), DCs (CD11c^{+}) and macrophages (CD11b^{hi} F4/80^{hi}) were evaluated by DAPI-exclusion and enumerated by adding a known number of fluorescent calibration particles to allow the determination of cell number. The number of live cells for each subtype were normalised relative to the number of corresponding cells in untreated (no Hla) controls co-cultured under identical conditions.

## In vitro time-lapse microscopy

Whole peritoneal lavages from MacGreen mice in which the GFP^{hi} cells are predominantly macrophages, were plated on to a FluoroDish™ (World Precision Instruments) immediately prior to addition of Hla (7.5μg/ml) and subsequent imaging. Cells were then imaged using a Leica SP500 confocal microscope equipped with resonant scanner in a humidified, 37°C chamber with 5% $CO_2$ for up to three hours. Differential interference contrast and fluorescence images were simultaneously collected using a 488nm laser, and data were analyzed and converted to movies using ImageJ64.

### General experimental design and statistical analysis

For animal experiments, littermates were randomly distributed to the treatment groups so that all groups were age and sex matched (no specific randomization or blinding protocol was used). No animals were excluded from the analysis. A single outlier sample from the 12 h PBS group (Fig. 1c) was excluded from analysis using the robust outlier detection method (Prism Software) based on pooled data from both PBS groups. Statistical analyses were performed using Prism software (GraphPad Software Inc.). Following experiments, where group size was adequately large, data were assessed for normality using a Kolmogrov-Smirnov test, and parametric or non-parametric tests applied as appropriate. Where data was demonstrated or suspected to deviate overtly from normality, or if there were unequal variances between groups, log transformation was applied prior to statistical analysis (as indicated in figure legends). Differences in *P*-value between treatment two groups were determined using a two-tailed unpaired t-test (parametric data). Alternatively, Mann-Whitney U test was used on non-parametric data. One-way ANOVA followed by either a Bonferroni or a Dunnett multiple comparison test (as described in figure legends) was used to determine statistical significance. Statistical difference was assumed if $P < 0.05$.

## Supplementary Material

Refer to Web version on PubMed Central for supplementary material.

## Acknowledgments

## References

1. Kolaczkowska E, Kubes P. Neutrophil recruitment and function in health and inflammation. Nat Rev Immunol. 2013; 13:159–175. [PubMed: 23435331]

2. Rigby KM, DeLeo FR. Neutrophils in innate host defense against *Staphylococcus aureus* infections. Semin Immunopathol. 2012; 34:237–259. [PubMed: 22080185]

3. Nourshargh S, Hordijk PL, Sixt M. Breaching multiple barriers: leukocyte motility through venular walls and the interstitium. Nat Rev Mol Cell Biol. 2010; 11:366–378. [PubMed: 20414258]

4. Kansas G. Selectins and their ligands: current concepts and controversies. Blood. 1996; 88:3259–3287. [PubMed: 8896391]

5. Laudanna C, Kim JY, Constantin G, Butcher E. Rapid leukocyte integrin activation by chemokines. Immunol Rev. 2002; 186:37–46. [PubMed: 12234360]

6. Massena S, et al. A chemotactic gradient sequestered on endothelial heparan sulfate induces directional intraluminal crawling of neutrophils. Blood. 2010; 116:1924–1931. [PubMed: 20530797]

7. Phillipson M, et al. Intraluminal crawling of neutrophils to emigration sites: a molecularly distinct process from adhesion in the recruitment cascade. J Exp Med. 2006; 203:2569–2575. [PubMed: 17116736]

8. Proebstl D, et al. Pericytes support neutrophil subendothelial cell crawling and breaching of venular walls *in vivo*. J Exp Med. 2012; 209:1219–1234. [PubMed: 22615129]

9. Bruns RR, Palade GE. Studies on blood capillaries. I. General organization of blood capillaries in muscle. J Cell Biol. 1968; 37:244–276. [PubMed: 5656394]

10. Hickey WF, Kimura H. Perivascular microglial cells of the CNS are bone marrow-derived and present antigen *in vivo*. Science. 1988; 239:290–292. [PubMed: 3276004]

11. Kim WK, et al. CD163 Identifies Perivascular Macrophages in Normal and Viral Encephalitic Brains and Potential Precursors to Perivascular Macrophages in Blood. Am J Pathol. 2006; 168:822–834. [PubMed: 16507898]

12. Chen GY, Nunez G. Sterile inflammation: sensing and reacting to damage. Nat Rev Immunol. 2010; 10:826–837. [PubMed: 21088683]

13. David MZ, Daum RS. Community-Associated Methicillin-Resistant *Staphylococcus aureus*: Epidemiology and Clinical Consequences of an Emerging Epidemic. Clin Microbiol Rev. 2010; 23:616–687. [PubMed: 20610826]

14. Noskin GA, et al. National Trends in *Staphylococcus aureus* Infection Rates: Impact on Economic Burden and Mortality over a 6-Year Period (1998–2003). Clin Infect Dis. 2007; 45:1132–1140. [PubMed: 17918074]

15. Boucher HW, Corey GR. Epidemiology of methicillin-resistant *Staphylococcus aureus*. Clin Infect Dis. 2008; 46 (Suppl 5):S344–349. [PubMed: 18462089]

16. Otto M. Basis of virulence in community-associated methicillin-resistant *Staphylococcus aureus*. Annu Rev Microbiol. 2010; 64:143–162. [PubMed: 20825344]

17. Bubeck Wardenburg J, Schneewind O. Vaccine protection against *Staphylococcus aureus* pneumonia. J Exp Med. 2008; 205:287–294. [PubMed: 18268041]

18. Kennedy AD, et al. Targeting of alpha-hemolysin by active or passive immunization decreases severity of USA300 skin infection in a mouse model. J Infect Dis. 2010; 202:1050–1058. [PubMed: 20726702]

19. Inoshima I, et al. A *Staphylococcus aureus* pore-forming toxin subverts the activity of ADAM10 to cause lethal infection in mice. Nat Med. 2011; 17:1310–1314. [PubMed: 21926978]

20. Inoshima N, Wang Y, Bubeck Wardenburg J. Genetic requirement for ADAM10 in severe *Staphylococcus aureus* skin infection. J Invest Dermatol. 2012; 132:1513–1516. [PubMed: 22377761]

21. Wilke GA, Wardenburg JB. Role of a disintegrin and metalloprotease 10 in *Staphylococcus aureus* α-hemolysin–mediated cellular injury. P Natl Acad Sci USA. 2010; 107:13473–13478.

22. Li JL, et al. Intravital multiphoton imaging of immune responses in the mouse ear skin. Nat Protoc. 2012; 7:221–234. [PubMed: 22240584]

23. Faust N, Varas F, Kelly LM, Heck S, Graf T. Insertion of enhanced green fluorescent protein into the lysozyme gene creates mice with green fluorescent granulocytes and macrophages. Blood. 2000; 96:719–726. [PubMed: 10887140]

24. Constantin G, et al. Chemokines trigger immediate beta2 integrin affinity and mobility changes: differential regulation and roles in lymphocyte arrest under flow. Immunity. 2000; 13:759–769. [PubMed: 11163192]

25. Peters NC, et al. In vivo imaging reveals an essential role for neutrophils in leishmaniasis transmitted by sand flies. Science. 2008; 321:970–974. [PubMed: 18703742]

26. Mempel TR, et al. Regulatory T Cells Reversibly Suppress Cytotoxic T Cell Function Independent of Effector Differentiation. Immunity. 2006; 25:129–141. [PubMed: 16860762]

27. Pollard JW. Trophic macrophages in development and disease. Nature reviews Immunology. 2009; 9:259–270.

28. Sasmono RT, et al. A macrophage colony-stimulating factor receptor-green fluorescent protein transgene is expressed throughout the mononuclear phagocyte system of the mouse. Blood. 2003; 101:1155–1163. [PubMed: 12393599]

29. Nishibu A, Ward BR, Boes M, Takashima A. Roles for IL-1 and TNFalpha in dynamic behavioral responses of Langerhans cells to topical hapten application. J Dermatol Sci. 2007; 45:23–30. [PubMed: 17123788]

30. Muzumdar MD, Tasic B, Miyamichi K, Li L, Luo L. A global double-fluorescent Cre reporter mouse. Genesis. 2007; 45:593–605. [PubMed: 17868096]

31. Ludwig A, et al. Metalloproteinase inhibitors for the disintegrin-like metalloproteinases ADAM10 and ADAM17 that differentially block constitutive and phorbol ester-inducible shedding of cell surface molecules. Comb Chem High Throughput Screen. 2005; 8:161–171. [PubMed: 15777180]

32. Lindquist RL, et al. Visualizing dendritic cell networks in vivo. Nat Immunol. 2004; 5:1243–1250. [PubMed: 15543150]

33. Sumaria N, et al. Cutaneous immunosurveillance by self-renewing dermal gamma delta T cells. J Exp Med. 2011; 208:505–518. [PubMed: 21339323]

34. Roediger B, et al. Cutaneous immunosurveillance and regulation of inflammation by group 2 innate lymphoid cells. Nat Immunol. 2013; 14:564–573. [PubMed: 23603794]

35. Stark K, et al. Capillary and arteriolar pericytes attract innate leukocytes exiting through venules and 'instruct' them with pattern-recognition and motility programs. Nat Immunol. 2013; 14:41–51. [PubMed: 23179077]

36. Sumagin R, Sarelius IH. Intercellular adhesion molecule-1 enrichment near tricellular endothelial junctions is preferentially associated with leukocyte transmigration and signals for reorganization of these junctions to accommodate leukocyte passage. J Immunol. 2010; 184:5242–5252. [PubMed: 20363969]

37. Wang S, et al. Venular basement membranes contain specific matrix protein low expression regions that act as exit points for emigrating neutrophils. J Exp Med. 2006; 203:1519–1532. [PubMed: 16754715]

38. Zaba LC, Fuentes-Duculan J, Steinman RM, Krueger JG, Lowes MA. Normal human dermis contains distinct populations of CD11c+BDCA-1+ dendritic cells and CD163+FXIIIA+ macrophages. J Clin Invest. 2007; 117:2517–2525. [PubMed: 17786242]

39. Ginhoux F, et al. Fate mapping analysis reveals that adult microglia derive from primitive macrophages. Science. 2010; 330:841–845. [PubMed: 20966214]

40. May AK, Gleason TG, Sawyer RG, Pruett TL. Contribution of Escherichia coli alpha-hemolysin to bacterial virulence and to intraperitoneal alterations in peritonitis. Infect Immun. 2000; 68:176–183. [PubMed: 10603385]

41. Foster TJ. Immune evasion by staphylococci. Nat Rev Microbiol. 2005; 3:948–958. [PubMed: 16322743]

42. Bhakdi S, Tranum-Jensen J. Alpha-toxin of *Staphylococcus aureus*. Microbiol Rev. 1991; 55:733–751. [PubMed: 1779933]

43. O'Reilly M, de Azavedo JCS, Kennedy S, Foster TJ. Inactivation of the alpha-haemolysin gene of *Staphylococcus aureus* 8325-4 by site-directed mutagenesis and studies on the expression of its haemolysins. Microb Pathogenesis. 1986; 1:125–138.

44. Paprotka K, Giese B, Fraunholz MJ. Codon-improved fluorescent proteins in investigation of *Staphylococcus aureus* host pathogen interactions. J Microbiol Meth. 2010; 83:82–86.

45. Ni L, et al. The *Staphylococcus aureus* pSK41 plasmid-encoded ArtA protein is a master regulator of plasmid transmission genes and contains a RHH motif used in alternate DNA-binding modes. Nucleic Acids Res. 2009; 37:6970–6983. [PubMed: 19759211]

46. Schenk S, Laddaga RA. Improved method for electroporation of *Staphylococcus aureus*. FEMS Microbiol Lett. 1992; 73:133–138. [PubMed: 1521761]

47. Mitchell AJ, et al. Technical advance: autofluorescence as a tool for myeloid cell analysis. J Leukoc Biol. 2010; 88:597–603. [PubMed: 20534703]

48. Ng LG, et al. Visualizing the neutrophil response to sterile tissue injury in mouse dermis reveals a three-phase cascade of events. J Invest Dermatol. 2011; 131:2058–2068. [PubMed: 21697893]

49. Lo Sardo V, et al. An evolutionary recent neuroepithelial cell adhesion function of huntingtin implicates ADAM10-Ncadherin. Nat Neurosci. 2012; 15:713–721. [PubMed: 22466506]
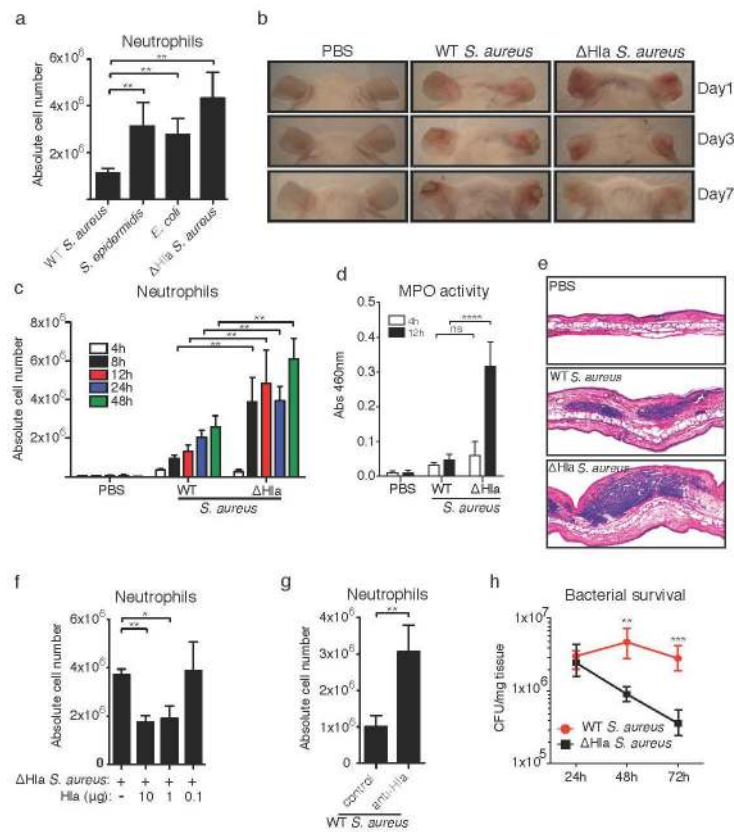
**Figure 1. Hla reduces neutrophil influx in *S. aureus* infected skin resulting in tissue necrosis and increased bacterial survival**

**(a)** Flow cytometry analysis of neutrophil influx in infected ears with indicated bacteria at 12h p.i. n=4 mice/group. **(b)** Clinical manifestations, and **(c)** neutrophil influx of ears infected with WT *S. aureus,* ΔHla *S. aureus* or after PBS injection at various timepoints mentioned in the figure. n=3 mice/group for PBS injected at each time point and for all groups at 48 hours; n=4 mice/group for WT & ΔHla *S. aureus* groups at 4h and 8h p.i.; n=5 mice/group for WT & ΔHla at 12h p.i.; n=6 mice/group WT & ΔHla at 24h p.i. **(d)** Myeloperoxidase activity in ear skin of mice either sham infected (PBS; n=3 mice/group) or infected with WT or ΔHla *S. aureus* at 4h (n=5 mice/group) and 12h (n=6 mice/group) p.i. A single outlier sample from the 12hr PBS group was excluded from analysis using the ROUT method. **(e)** Representative haematoxylin and eosin stained ear sections obtained from mice infected with PBS (n=3 mice/group), WT or ΔHla *S. aureus* at 6h p.i. (n=6 mice/group). **(f)** Neutrophil influx in ears of mice at 12h p.i. with concomitant injection of ΔHla *S. aureus* and purified Hla (n=4 mice/group). **(g)** Neutrophil influx in ears at 12h p.i. with WT *S. aureus* in mice pretreated with control serum or anti-Hla serum (n=4 mice/group). **(h)** Bacterial load (CFUs) of infected ears at indicated time points (n=4 mice/group). Bars represent mean±SD. All data are representative of at least 2 independent experiments except for (**e**), which is from a single experiment. Statistical analysis was performed on log-transformed data as follows: (**a** and **f**) one-way ANOVA with Bonferroni's multiple comparison test; (**c, d** and **h**) two-way ANOVA with Bonferroni test; (**g**) Student's two-

tailed unpaired t-test was used to determine the *P*-value. \*\**P*<0.01; \*\*\**P*<0.001; \*\*\*\**P*<0.0001; n.s, not significant.
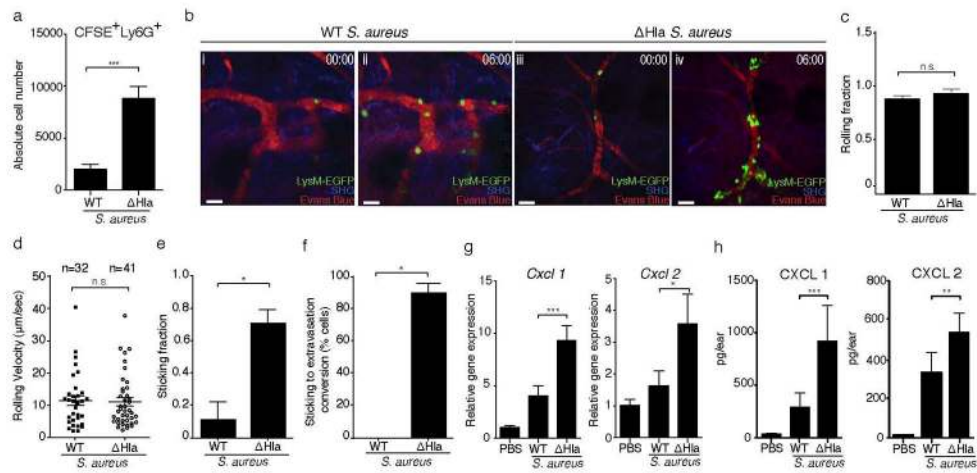
**Figure 2. Hla-mediated prevention of neutrophil extravasation during cutaneous *S. aureus* infection**

(**a**) Numbers of CFSE⁺Ly6G⁺ neutrophils at 12h p.i., determined by flow cytometry, in WT and ΔHla *S. aureus* infected ears. CFSE-labeled bone marrow cells were transferred at 10h p.i. Bars represent mean±SD; n=3 mice/group. (**b**) Intravital multi-photon microscopy showing the increased adhesion and extravasation of adoptively transferred LysM-EGFP⁺ neutrophils in ΔHla *S. aureus* (iii,iv) as compared to WT *S. aureus* (i,ii) infected ear dermis. 00:00, min:sec. SHG, Second harmonic generation. Scale bar, 30μm. Neutrophil rolling fractions (**c**), mean rolling velocities (**d**) and sticking fractions (**e**) in dermal blood vessels of mice infected with WT *S. aureus* or ΔHla *S. aureus*. (**f**) Conversion of neutrophil sticking to extravasation in the blood vessels of mice infected with WT *S. aureus* or ΔHla *S. aureus*. n, number of events analyzed per group (cumulative from 3 mice/group). Imaging data shown in (**b–f**) were from one out of two experiments with n=3 mice/group each. More than 10 vessels of diameters ranging between 10–30μm were included in these analyses for each treatment group. Bars represent mean±SEM. (**g**) Relative *Cxcl1* and *Cxcl2* mRNA levels as determined by RT-qPCR (PBS: n=3 mice/group; WT and ΔHla *S. aureus*: n=5 mice/group; mean±SD) and (**h**) protein levels in mice injected with PBS (n=4) WT *S. aureus* (n=7) or ΔHla *S. aureus* (n=8). Bars represent mean±SD. Neutrophil numbers (**a**) were analyzed using a two-tailed Student's t-test on log-transformed data. Imaging data were analyzed using either a two-tailed (**c** and **d**) or one-tailed (**e** and **f**) Mann-Whitney U test. Chemokine data (**g** and **h**) were analyzed using a one-way ANOVA and Bonferroni's post-test following log transformation. *$P<0.05$; **$P<0.01$; ***$P<0.001$. n.s., not significant. Unless otherwise stated data are representative of at least two independent experiments.
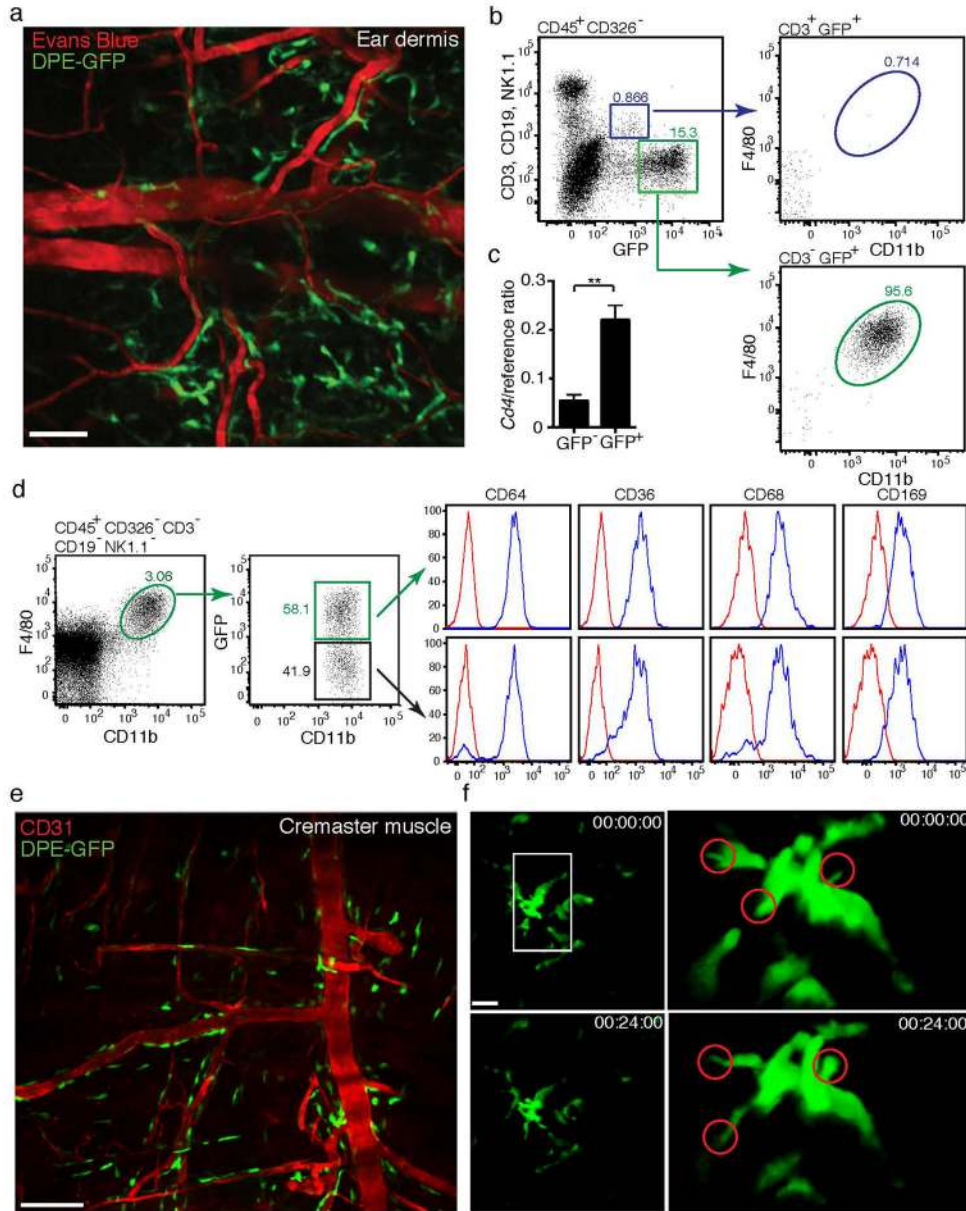
**Figure 3. Perivascular macrophages can be identified in transgenic DPE-GFP mice**

(a) Multi-photon imaging of dermis of DPE-GFP mice showing presence of GFP$^+$ cells with dendritic morphology apposed to dermal vessels (delineated by Evans Blue). Image is representative of more than 3 independent experiments. (b) Flow cytometric analysis of GFP$^+$ cells from ear skin of DPE-GFP mice, showing expression of GFP by CD11b$^-$F4/80$^-$CD3$^+$ αβ T cells and CD11b$^+$F4/80$^+$ CD3$^-$ macrophages (cells were pooled from 3 mice/experiment – representative of two independent experiments). (c) CD4 mRNA expression by sorted GFP$^+$ and GFP$^-$ CD45$^+$CD11b$^+$F4/80$^+$ macrophages. Bars indicate mean±SEM of 4 independent experiments. Statistical significance was determined using a two-tailed unpaired t-test on log transformed data. (d) Phenotypic analysis of GFP$^+$ and GFP$^-$ macrophages in DPE-GFP mice (cells pooled from 3 mice/experiment –

representative of two independent experiments). **(e)** Confocal imaging of GFP[+] macrophages associated with post-capillary venules in cremaster muscle. **(f)** Multi-photon imaging of PVM in ear dermis of DPE-GFP mice showing extension and retraction of dendrites. Single cell images have been rotated to better represent dendritic behavior (circled). 00:00:00, hr:min:sec. Imaging data are representative of a minimum of 3 animals (**a, e, f**) in independent experiments. \*\**P*<0.01.
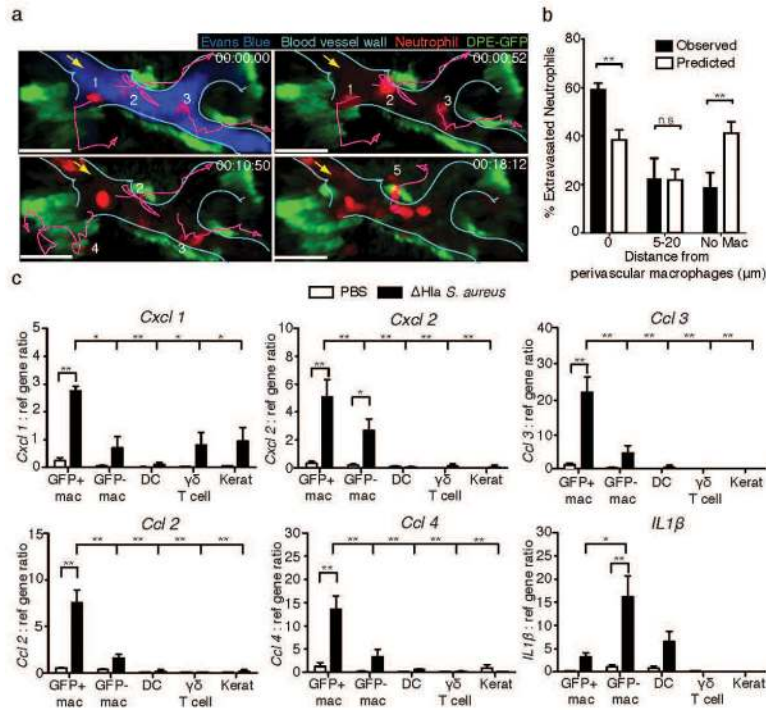
**Figure 4. Neutrophils extravasate adjacent to perivascular macrophages in inflamed dermal vessels**

(**a**) Time-lapse intravital multi-photon imaging of ear dermis of DPE-GFP mice infected with ΔHla *S. aureus* depicting the adherence and extravasation of adoptively transferred neutrophils isolated from mT/mG mice (red, numbered 1–5) in close proximity to perivascular macrophages (green). Lines (purple) represent migration tracks of selected neutrophils (red) and the arrow (yellow) represents the direction of blood flow in the vessel (cyan). 00:00:00, hr:min:sec. Scale bar 30μm (**b**) Statistical analysis of neutrophil extravasation site with respect to perivascular macrophages. Numbers of neutrophils extravasating at theoretical/random (white bars) or observed (black bars) distances from GFP⁺ perivascular macrophages within the same vessels. Data represents 45 total extravasation events from 5 mice pooled from 2 independent experiments. Bars represent mean±SEM. Statistical significance was determined by two-way ANOVA with a Bonferroni's multiple comparisons test. (**c**) Relative gene expression by the indicated cell populations (GFP⁺ or GFP⁻ macrophages, dendritic cells (DC), γδ T cells and keratinocytes) isolated from ears of ΔHla *S. aureus* infected or control (PBS) treated mice at 6h p.i. Data shown are mean±SEM of 3 independent experiments. *P*-values were calculated using two-way ANOVA with a Bonferroni's multiple comparison test (between treatment comparisons) and one-way ANOVA with Dunnett's multiple comparison test (determination of differences between GFP⁺ macrophages and other cell types from infected animals), *$P<0.05$; **$P<0.01$. n.s., not significant.
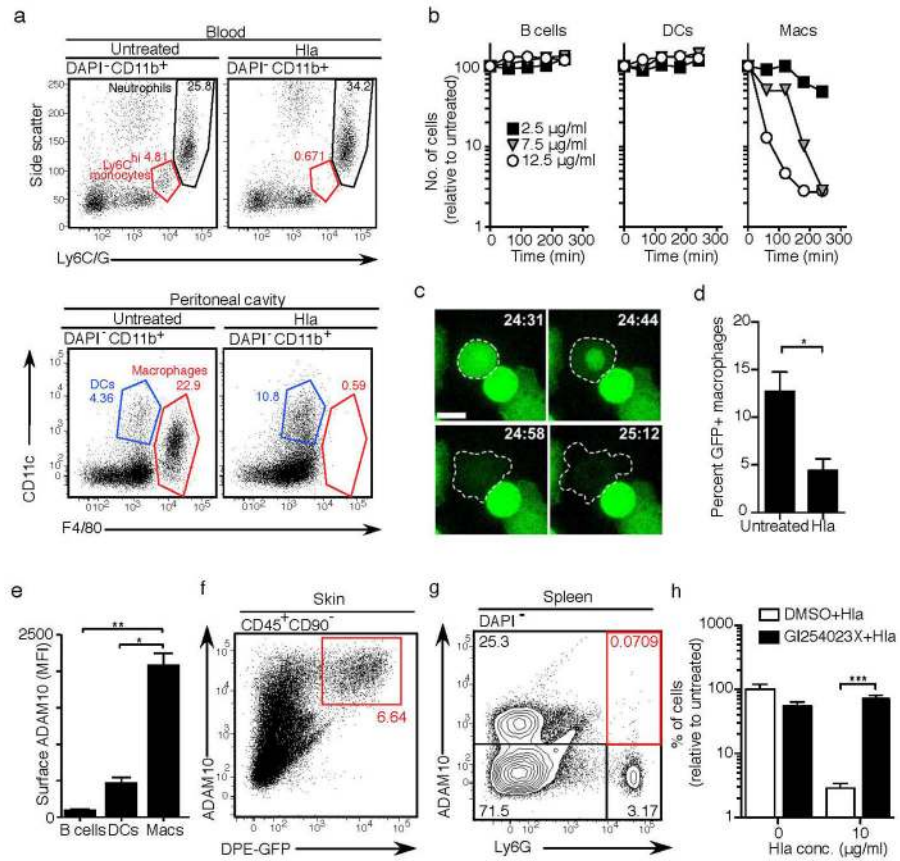
**Figure 5. Hla specifically lyses ADAM10$^+$ macrophages**
(**a**) Leukocytes were isolated from peripheral blood or the peritoneal cavity and incubated with Hla (7.5 μg/ml) for 3h. Cell viability was assessed by flow cytometry. Data are representative of 3 mice from one of two experiments (blood) or more than 10 experiments (peritoneal cells). (**b**) Specific death of peritoneal macrophages, but not B cells or dendritic cells, in the presence of indicated concentrations of Hla. Symbols represent individual values from a single experiment using cells pooled from 3 mice. Data are representative of more than 10 independent experiments using a range of Hla concentrations and times. (**c**) *In vitro* live imaging of peritoneal macrophage cell death in the presence of Hla (7.5 μg/ml). Scale bar 10μm. 00:00, min:sec. Images are representative of two independent experiments using cells isolated from *Csf1r*-EGFP mice. (**d**) Death of GFP$^+$ macrophages harvested from the skin of DPE-GFP mice following *in vitro* culture in the presence of Hla (12.5 μg/ml). Data are expressed as a percentage of total CD45$^+$ cells and are representative of 2 independent experiments (n=4 mice/group). (**e**) ADAM10 expression levels on peritoneal leukocyte populations as determined by flow cytometry. Data are representative of 2 independent experiments (n=3 mice/group). (**f**) High level of ADAM10 expression by DPE-GFP$^+$ cells from the skin. Data are from an individual mouse and are representative of 4 independent experiments using cells either from individual animals or pooled from 3 mice. (**g**) Absence of ADAM10 expression by neutrophils (Ly6G$^+$ cells) in spleen. Data shown are from a single mouse in one of two experiments with a total of n=4 animals. (**h**) GI254023X mediated protection of peritoneal macrophages from Hla-induced lysis. One out of three

experiments using cells pooled from 3 mice performed in quadruplicate is shown. Bars indicate mean±SD of technical replicates. MFI = geometric mean fluorescence intensity. Statistical analysis was performed as follows: (**d**) two-tailed t-test; (**e**) one-way ANOVA or (**h**) two-way ANOVA with Bonferroni's multiple comparison test on log transformed data. *$P$<0.05; **$P$<0.01; ***$P$<0.0001.
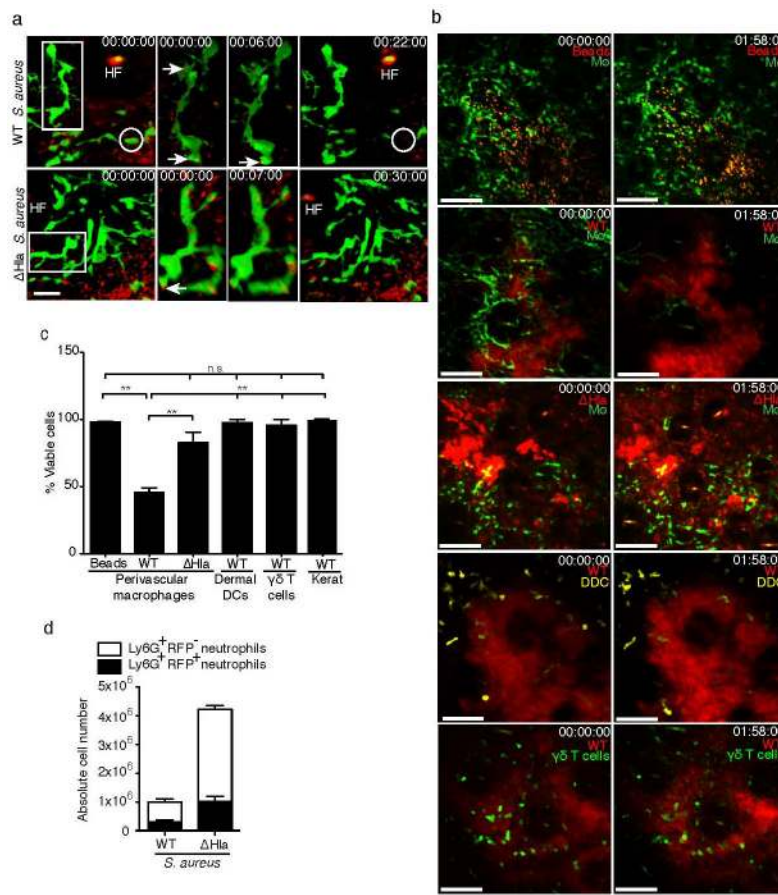
**Figure 6. Specific lysis of DPE-GFP$^+$ PVM by ΔHla *S. aureus in vivo***
**(a)** Intravital multi-photon images showing phagocytosis of WT and ΔHla *S. aureus* (red) by DPE-GFP$^+$ macrophages (green). Single cell images have been rotated to highlight bacterial uptake (arrows). A GFP$^+$ macrophage that is lysed during the course of the video is circled. HF, autofluorescent hair follicle. Data are representative of n=2 mice/group from one of two independent experiments. (**b**) Intravital multi-photon images of ear skin of DPE-GFP mice (macrophage, MΦ) 2h p.i. with RFP-expressing WT *S. aureus,* ΔHla *S. aureus* or fluorescent beads. Effects of WT *S. aureus* infection in ear skin on dermal dendritic cells (CD11c-YFP$^+$) or γδ T cells (CXCR6-GFP$^+$) are also shown. Scale bar, 60 μm. Numbers represent time in hr:min:sec, Pooled data from 2 independent experiments are shown. n=6 for PVM from DPE-GFP mice infected with WT *S. aureus* and n=3 mice for all other groups**. (c)** Graph representing quantitative analysis of macrophage, DC, and T cells as shown in (b). Keratinocyte death (Kerat) was analyzed in mT/mG mice using WT *S. aureus*. Bars represent mean±SEM. Statistical analysis was performed using one-way ANOVA and Bonferroni's multiple comparison test. **(d)** absolute numbers of neutrophils with phagocytosed RFP-expressing WT or ΔHla *S. aureus* in the skin 12h p.i. Data show mean ±SD of 3 mice/group and are representative of two independent experiments. Error bars indicate SD. \*\**P*<0.01; n.s., not significant.